South Atlantic response to El Niño–Southern Oscillation induced climate variability in an ocean general circulation model

F. Colberg and C. J. C. Reason
Oceanography Department, University of Cape Town, Rondebosch, South Africa

K. Rodgers
Laboratoire d'Oceanographie Dynamique et de Climatologie, CNRS, University Paris VI, Paris, France

Received 29 January 2004; revised 16 August 2004; accepted 28 September 2004; published 14 December 2004.

[1] The response of the South Atlantic Ocean to El Niño-Southern Oscillation (ENSO) is investigated by means of an ocean general circulation model (ORCA2) forced with National Centers for Environmental Prediction (NCEP) reanalyses for the 1948–1999 period. Seasonal ENSO composites suggest that the ENSO-induced wind anomalies play a major role in driving upper ocean temperatures by altering the net surface heat fluxes, the meridional Ekman heat transport, and Ekman pumping. Model diagnostics indicate that the Ekman heat transport changes are in better agreement with the upper ocean temperature anomalies during the first half of the ENSO event whereas, in the latter half, the surface heat flux anomalies agree better. In general, the atmospheric forcing tends to lead to a coherent ocean response with a time lag of about one season. Subsurface temperatures evolve more slowly in response to ENSO forcing than the upper ocean. They receive time-filtered ENSO signals from mainly Ekman pumping (suction) and variations in thermocline depth that result in the poleward and equatorward margins of the subtropical gyre exhibiting temperature anomalies of the same sign but opposite to those in the central regions of the gyre. *INDEX TERMS:* 3309 Meteorology and Atmospheric Dynamics: Climatology (1620); 3339 Meteorology and Atmospheric Dynamics: Ocean/atmosphere interactions (0312, 4504); 4522 Oceanography: Physical: El Nino; *KEYWORDS:* ENSO, modeling, South Atlantic variability

Citation: Colberg, F., C. J. C. Reason, and K. Rodgers (2004), South Atlantic response to El Niño–Southern Oscillation induced climate variability in an ocean general circulation model, *J. Geophys. Res.*, *109*, C12015, doi:10.1029/2004JC002301.

1. Introduction

[2] South Atlantic Ocean variability plays an important role in affecting both global and regional climate. The former results from its unique geographical location connecting the Indian Ocean to the North Atlantic Ocean. Thus this basin acts as an important part of the thermohaline circulation [*Schmitz*, 1995]. The latter arises since sea surface temperature (SST) patterns in the South Atlantic interact with the atmosphere, leading to rainfall variability over neighboring countries [*Rouault et al.*, 2003; *Robertson et al.*, 2003]. *Reason et al.* [2002] present evidence of rainfall variability over the southwestern Cape of South Africa in the context of an enhanced meridional SST gradient in the South Atlantic and subtropical-midlatitude SST anomalies in the southwest and central parts of the basin. *Robertson et al.* [2003] found evidence of an atmospheric response to oceanic SST anomalies in the tropics and subtropics of the South Atlantic in an AGCM. The existence of warm events in the eastern Atlantic and the impact on fish stocks along the western African coast has been examined by *Binet et al.* [2001] and *Gammelsrod et al.* [1998].

0148-0227/04/2004JC002301

[3] The South Atlantic Ocean experiences significant variability on interannual to multidecadal timescales [e.g., *Venegas et al.*, 1996, 1997, 1998; *Reason*, 2000; *Wainer and Venegas*, 2001; *Palastanga et al.*, 2002; *Reason et al.*, 2002]. Some SST variability occurs during El Niño and La Niña events, implying a relationship with ENSO as a possible forcing. This implication gains support from *Venegas et al.* [1996] where the third SVD mode between SST anomalies and pressure anomalies of the South Atlantic is highly correlated with ENSO. The associated spatial pattern suggests a north-south displacement of the subtropical anticyclone implying gyre modifications due to ENSO. Analyses of SST anomalies in the western South Atlantic [*Lentini et al.*, 2001] show that warm (cold) phases of ENSO are connected to northward (southward) extensions of cold (warm) water a year later in that region. Other studies such as *Melice and Servain* [2003] find correlations between the tropical Atlantic meridional SST gradient (TAMG) and the SOI, again suggesting connections between ENSO and the South Atlantic region. However, other South Atlantic modes may occur due to local atmospheric forcing, coupled ocean-atmosphere modes, and internal basin modes.

[4] A recent study by *Palastanga et al.* [2002] shows that various modes of variability in the South Atlantic may depend on the degree of data coverage in certain areas as

well as on the statistical tools used. These results show that there is still a lot of work needed in order to understand South Atlantic variability. Both analysis of available observations and output from ocean and coupled models are necessary in order to better understand the variability of the region. To date, not many attempts have been made to investigate South Atlantic Ocean variability using models. *Wainer and Venegas* [2001] detected South Atlantic multidecadal variability in the NCAR Climate System model in a 300-year integration model run and found significant oscillations of a 25- to 30-year period. Observational data show a similar signal indicating that models are indeed a useful tool in order to detect climate variability. Furthermore, models offer a more complete picture of what is happening in the oceans since they supply not only information about the surface but also allow investigation of subsurface features such as Kelvin waves which are thought to be important for warm and cool events in the northern Benguela Current region [*Florenchie et al.*, 2003].

[5] In this study, ENSO composites derived from an ocean general circulation model (OGCM) will be presented in an attempt to understand the evolution of the ENSO signal over the South Atlantic and the associated mechanisms in this basin. In particular, the model will be used to investigate the potential linkages between subsurface ocean processes and the evolution of SST anomalies over the South Atlantic during ENSO.

2. Model Description

[6] The OGCM used is the ORCA2 model, which is the global version of the Ocean Parallelise [*Madec et al.*, 1998]. The global domain extends from 78°S to 90°N. The bottom topography and coastlines are derived from *Smith and Sandwell*'s [1997] data complemented by values from the $5' \times 5'$ ETOPO 5 data set at the northernmost latitudes. Lateral mixing is oriented isopycnically, and the eddy parameterization scheme of *Gent and McWilliams* [1990] is applied poleward of 10° in both hemispheres. Vertical mixing is achieved using the TKE scheme of *Blanke and Delecluse* [1993].

[7] The zonal resolution is 2°, the meridional resolution decreases from 0.5° at the equator to 2° × cos(latitude) poleward of 20° in either hemisphere. The model grid is tripolar, with two poles in the Northern Hemisphere (over North America and Siberia) and one centered over Antarctica. In the vertical, the model consists of 30 layers, with 20 of these layers in the upper 500 m. Thus the model has appropriate resolution to represent both equatorial circulation and upper ocean processes. A sea ice model representing both thermodynamic and dynamic processes is coupled to the OGCM [*Fichefet and Morales Maqueda*, 1997].

[8] The OGCM model is initialized with *Levitus* [1998] temperature and salinity values. The surface boundary condition is a bulk mixed layer that receives the air temperature, air humidity, total cloudiness, surface pressure, and surface wind speed (from the NCEP reanalyses) from which surface heat fluxes are calculated. Since the NCEP reanalyses use observed SST as a lower boundary condition and observations in the South Atlantic are relatively sparse before 1958, the quality of these reanalyses could be questioned. However, *Sterl and Hazeleger* [2003] have discussed this problem in detail and come to the conclusion that using the reanalyses in the South Atlantic is reasonable.

[9] A 200-year spin-up with a restoring boundary condition on surface salinity (2-month timescale) and climatological wind and heat flux forcing has been performed [*Madec et al.*, 1998]. A salinity flux correction for the 1948–1999 run has been done by applying the annual mean fluxes from the last 50 years to the interannually varying NCEP runs. Salinity variability may affect the ocean circulation due to density changes, which may then lead to pressure gradient changes and anomalous currents. Given the relatively poor quality of available freshwater flux data, this approach is necessary and is also frequently used by other modelers (e.g., POCM [*Stammer et al.*, 1996]). The model output analyzed in this paper consists of a 24.33-day average (i.e., 15 outputs per year) for each variable for the 1948–1999 period.

3. Data and Methods

[10] In this study, ORCA2 model data for sea surface temperature (SST), temperature at 55 m depth (ST55), and temperature at 215 m depth (ST215) are analyzed for the South Atlantic region. In addition, we examine SST from the GISST data set version 3.0 [*Rayner et al.*, 1996], with a zonal and meridional resolution of 1°.

[11] The generation and subsequent evolution of the model temperature anomalies during ENSO are investigated by examining the following variables: (1) NCEP reanalyses [*Kalnay et al.*, 1996] sea level pressure (SLP); (2) thermocline depth, which is assumed to be the depth of the strongest vertical gradient in temperature; (3) horizontal Ekman heat transport, calculated after *Levitus* [1987] using

$$F = -\frac{Cp(T-\theta)\tau}{fz}$$

where Cp is the specific heat capacity (4187 $JKg^{-1}\,K^{-1}$), T is the surface potential temperature, θ is the vertical mean temperature of the whole water column, τ is the wind stress, f is the Coriolis parameter, and z the depth of the water column; (4) Ekman pumping, using

$$Ep = \frac{1}{\rho_0 f}\left\{\frac{\partial \tau_y}{\partial x} - \frac{\partial \tau_x}{\partial y}\right\}$$

where ρ_0 is the potential density (1025 kg/m^3), f is the Coriolis parameter, and τ_{xy} is the wind stress in x and y direction, respectively; (5) calculations of the expected temperature changes due to surface heat flux forcing have been made using

$$\frac{dT}{dt} = \left(\frac{\mathrm{NHFL}}{Cp \cdot \rho \cdot \mathrm{DML}}\right),$$

where NHFL is the net downward heat flux (Wm^{-2}), DML is the depth of the mixed layer (m) calculated as the level

Table 1. El Niño and La Niña Years Chosen Such That the 5-Month Running Average of the Niño 3.4 Index Exceeds 0.4°C (−0.4°C) for at Least Six Consecutive Months

	Years
El Niño	1957/1958, 1963/1964, 1965/1966, 1972/1973, 1982/1983, 1986/1987, 1997/1998
La Niña	1949/1950, 1954/1955, 1955/1956, 1970/1971, 1973/1974, 1975/1976, 1988/1989, 1995/1996, 1998/1999

where the density increases by 0.01 kg m^{-3} from the surface, *Cp* is the specific heat capacity (4187 JKg^{-1} K^{-1}), ρ is the density of seawater (an average value of 1027 kg m^{-3} has been taken) and *T* is the temperature (K); and (6) combined wind stress anomaly and climatology pattern (CWP) has been defined, as follows:

[12] Let $x = \bar{\tau} \cdot \tau'$, with $\bar{\tau}$ denoting the wind stress climatology and τ' denoting the wind stress anomaly, and let

$$y(x) = 1 \; for \; x > 0$$
$$y(x) = -1 \; for \; x < 0$$

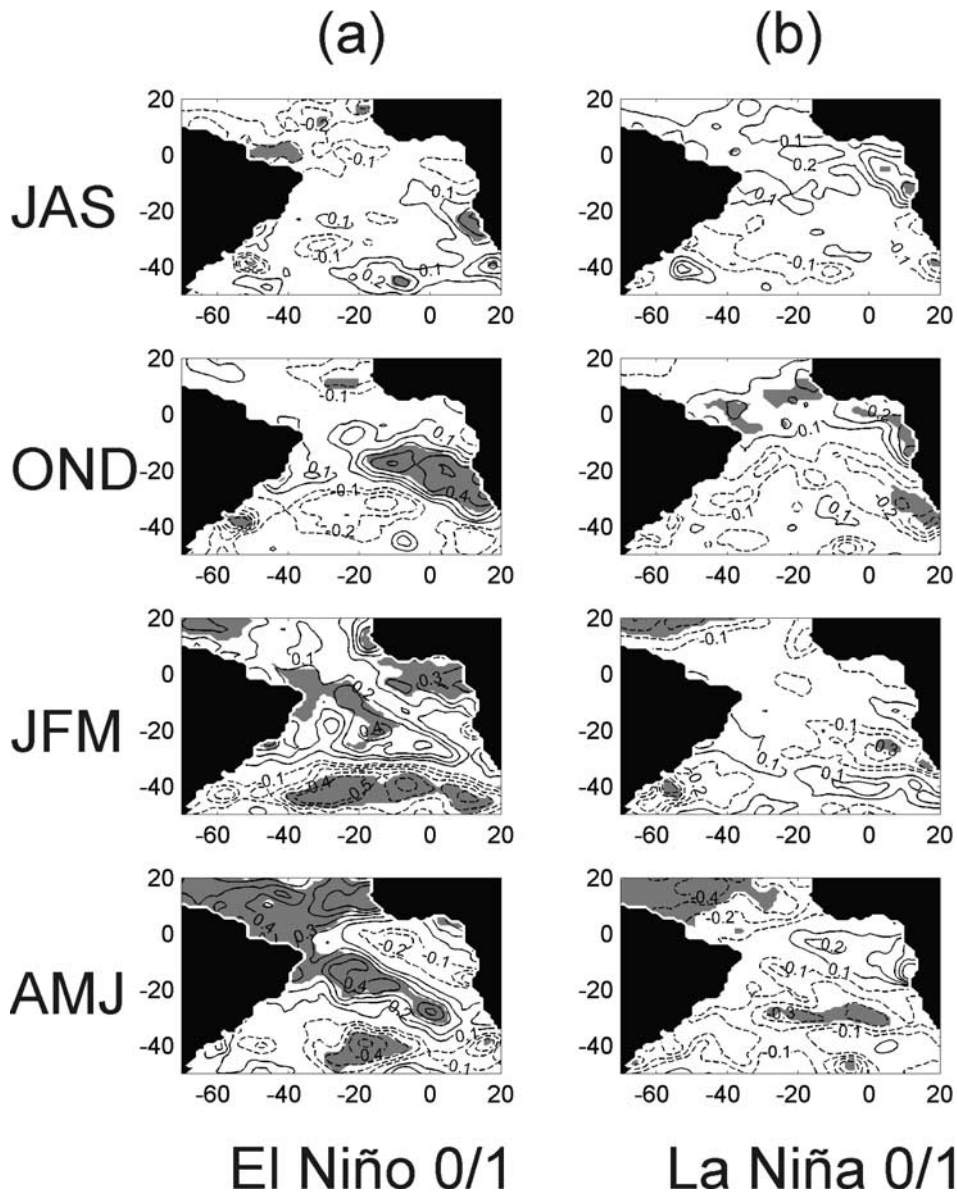

Figure 1. Seasonal composites of UKMO GISST 3.0 SSTA for the (a) El Niño phase and (b) La Niña phase from austral winter of the onset year through to austral autumn of the following year. Dashed (solid) contours denote negative (positive) values. Significant *t*-test areas at the 90% level are shaded gray (black and white version), and are marked by thick dashed lines (color version). The contour interval is 0.1°C. The zero contour line is omitted. A color scale in °C is given on the right for each individual contour plot (color version). See color version of this figure in the HTML.

then $cwp = -|\tau'| \cdot y$, with *cwp* being the combined wind stress anomaly and climatology pattern. Thus areas with positive (negative) values of CWP correspond to reduced (enhanced) winds and therefore may lead to positive (negative) surface temperature anomalies via thermodynamic effects such as changes in the net surface heat fluxes.

[13] A simple *t*-test has been applied to all seasonal fields shown in this paper. No *t*-test has been applied to the fields showing yearly means because, due to averaging, there are only small areas that are significant at the 90% confidence level.

[14] Since the model is forced with NCEP reanalysis, the data range covers the years between 1948 and 1999. The analyzed region ranges from 20°N to 50°S and from 70°W to 20°E. The seasonal anomalies shown below are derived by subtracting the climatological mean (52 years) from the values for that season. All derived anomalies are then detrended, by subtracting the linear trend from the anomalies.

[15] In order to identify individual ENSO events, the Niño 3.4 Index has been used and applied to both the ORCA model SST anomalies and the GISST 3.0 SST anomalies. El Niño (La Niña) events are identified if the 5-month running average of the Niño 3.4 Index exceeds 0.4°C (−0.4°C) for at least six consecutive months. Table 1 lists the events that result from this selection method as El Niño (La Niña) and El Niño +1 (La Niña +1) years. The former refers to years when the Niño 3.4 SST anomaly first appears while the +1 years refer to the following years (i.e., the mature phase years).

[16] To validate the ORCA model output, seasonal composites of SST anomalies (shown in the second column of Figure 3 (in section 4.1.2) for El Niño and Figure 5 (in section 4.2.1) for La Niña years) were compared to the GISST 3.0 SSTA (Figure 1) and to the NCEP surface air temperature (not shown). There is generally good agreement between the GISST SST anomalies (Figure 1) and the ORCA SST anomalies (see Figures 3 and 5, second column) for each of the composite years in terms of spatial pattern, although smaller features displayed by the GISST SST anomalies are not always captured by ORCA. This may partly reflect the higher resolution of the GISST data set (apart from the equatorial region) compared to ORCA.

[17] The similarity of the ORCA SST anomalies to the NCEP surface air temperature anomalies (not shown) is expected and reflects the nature of the model forcing using surface air temperature in the surface heat flux forcing, which implies a nudging of SST anomalies toward observed air temperatures. However, there are differences in the spatial patterns as well as in the magnitudes. Generally, the NCEP surface air temperatures are somewhat stronger than the ORCA SST anomalies.

[18] When assessing the accuracy of the ORCA SST, two points should be emphasized. First, the spatial distribution as well as the magnitudes of ORCA SST anomalies seem to be able to capture the seasonal evolution of the large-scale interannual anomalies like El Niño or La Niña patterns. Second, the upper model level is not optimal for showing the ability of ORCA to represent temperature variations due to the way the heat flux boundary condition is applied. Although the bulk mixed layer is trying to represent what is actually being forced from the atmospheric boundary layer without providing SST information, by prescribing atmospheric temperature values the upper ocean level is nudged toward observed temperatures. Thus, looking at subsurface temperatures is appropriate and, in the following, we present anomalies at the surface, at 55-m (near mixed layer base), and at 215-m (near thermocline) levels.

4. South Atlantic Response to ENSO Events

[19] In the following section, the response of the South Atlantic to ENSO events will be discussed by looking at seasonal composites. Upper ocean temperature anomalies are examined from JAS of the ENSO year to AMJ following the mature phase (ENSO +1 year). Sea level pressure, wind stress, and variables that are a function of these (CWP, meridional Ekman heat flux) and net surface heat fluxes are examined from AMJ of the ENSO year to JFM of the following year (i.e., the mature phase). The reason for so doing is that we find that upper ocean temperature anomalies during ENSO are mainly the result of the atmospheric forcing and respond to them with a time lag of roughly one season.

[20] Unfortunately, latent heat fluxes from ORCA are not available; hence we have instead examined the NCEP values (not shown). These fluxes are generally consistent with the model upper ocean temperatures, with the latter lagging the flux by one season similar to what we show below for the wind and net surface heat flux. Furthermore, the NCEP latent heat fluxes agree well with the net downward heat flux anomalies shown below, suggesting that the latent heat flux is the dominant factor in the surface heat budget.

[21] During El Niño, the upper ocean temperature anomalies in the South Atlantic generally start off negative (weakly positive) in the tropics (midlatitudes) and warm (cool) by the mature phase and then weaken or, in some areas, take the opposite sign during the following austral autumn. The La Niña anomalies are roughly the reverse. Evidence is presented below that these changes in temperature are caused by anomalous wind stresses, that lead to changes in net surface heat fluxes and Ekman heat transports. For the El Niño phase, a reduced tropical southward and enhanced midlatitude northward heat transport is apparent, consistent with the warming in the tropics and parts of the subtropics and the cooling in the midlatitudes. For the La Niña phase the reverse seems to occur, again consistent with the temperature anomalies.

4.1. Detailed Analysis of the El Niño-Induced Anomalies

4.1.1. Upper Ocean Temperatures (SST and ST55)

[22] Figures 3b and 3c in section 4.1.2 show the model surface (SST) and 55-m-depth (ST55) temperature anomalies. During JAS, significant (at the 90% level) warming is apparent in the Benguela current region, and this extends northwestward and peaks during the following season (OND). By OND, areas of the western subtropics/midlatitudes show cold anomalies, and this NE/SW pat-

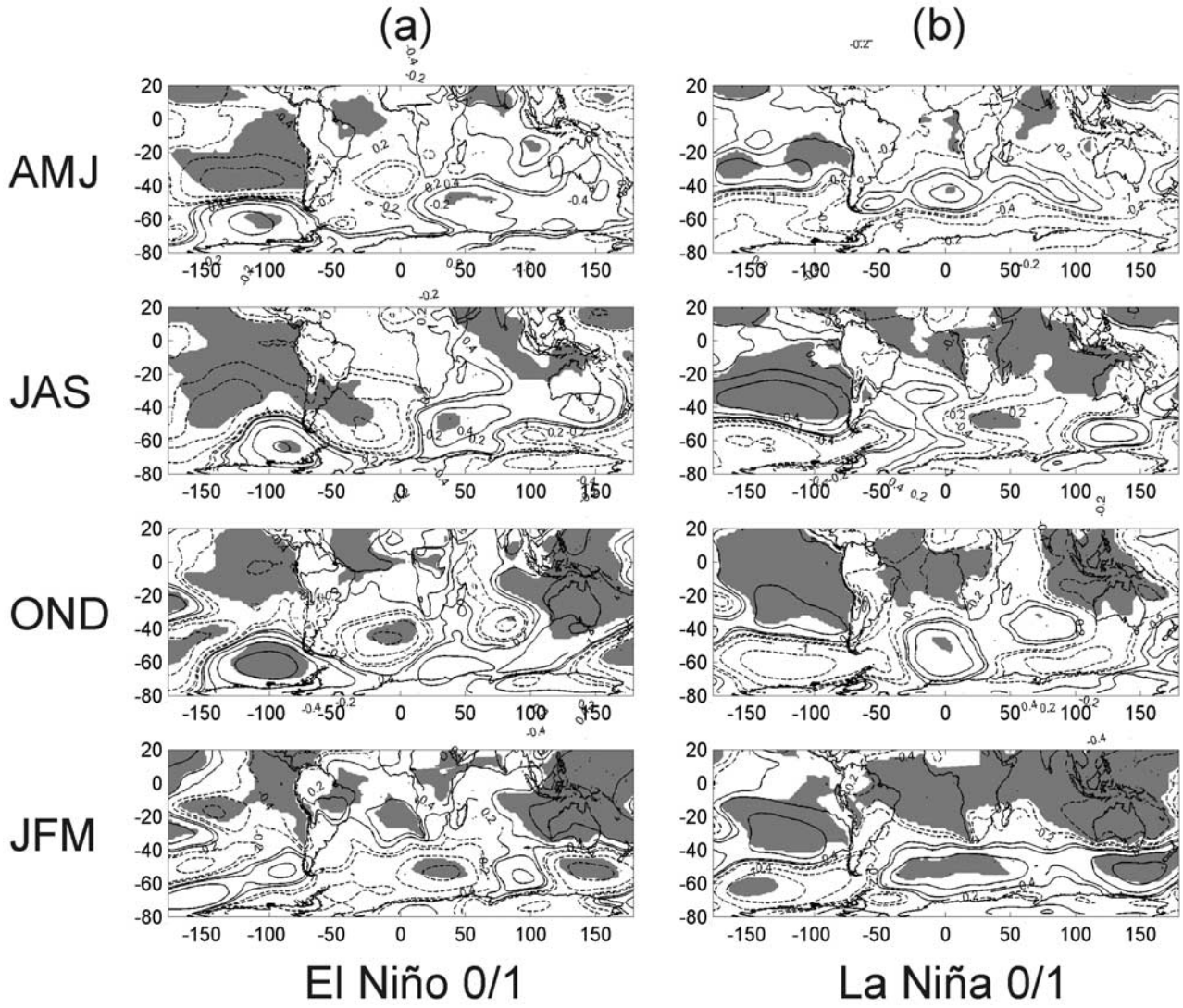

Figure 2. Seasonal composites of SLPA for the (a) El Niño phase and (b) La Niña phase. Dashed (solid) contours denote negative (positive) values. Significant *t*-test areas at the 90% level are shaded. The given contour lines are 4, 2, 1, 0.4, and 0.2 hPa for positive and negative values, respectively.

tern evolves to a more N/S oriented warm/cool anomaly by JFM. A larger tropical North Atlantic area shows warm anomalies in the following AMJ with a band of subtropical warming also apparent across the South Atlantic. The South Atlantic central midlatitudes remain cool, but weaker than JFM, and the eastern equatorial and tropical South Atlantic has evolved toward cool anomalies.

4.1.2. Sea Level Pressure (SLP) and CWP

[23] Figure 2a shows global SLP anomalies for the El Niño episode with the well-known ENSO patterns over the tropical Indo-Pacific evident. Over the South Atlantic, a negative anomaly is apparent in the subtropics/midlatitudes which strengthens in JAS, and weakens by JFM. These anomalies therefore modulate the subtropical anticyclone and the midlatitude westerlies. This anomaly pattern is likely part of the Pacific South American wave train pattern caused by atmospheric Rossby waves emanating from ENSO-modulated atmospheric convection in the Indo-Pacific region [*Mo and Paegle*, 2001].

[24] During AMJ, the reduced South Atlantic subtropical anticyclone leads to a weakening of the trades and the westerlies over the basin. The corresponding CWP plot (Figure 3a) shows the resulting enhanced and reduced wind stress anomalies. These areas more or less correspond to those of cooling (warming) seen one season later (JAS) in the upper ocean temperature fields (Figures 3b and 3c). During the following JAS, the negative SLP anomaly strengthens and moves farther to the southwest and is now significant at the 90% level. As a result, the westerlies are enhanced, but the trades are still reduced (Figure 3a), and the temperature anomalies (Figures 3b and 3c) essentially reflect this.

[25] The negative SLP anomaly weakens and moves northeast in OND, as the positive pressure anomalies west of Drake Passage and the neighboring Southern Ocean strengthen, and positive anomalies become apparent in the tropical South Atlantic. As a result, the westerlies are still enhanced over the South Atlantic, and the trades imme-

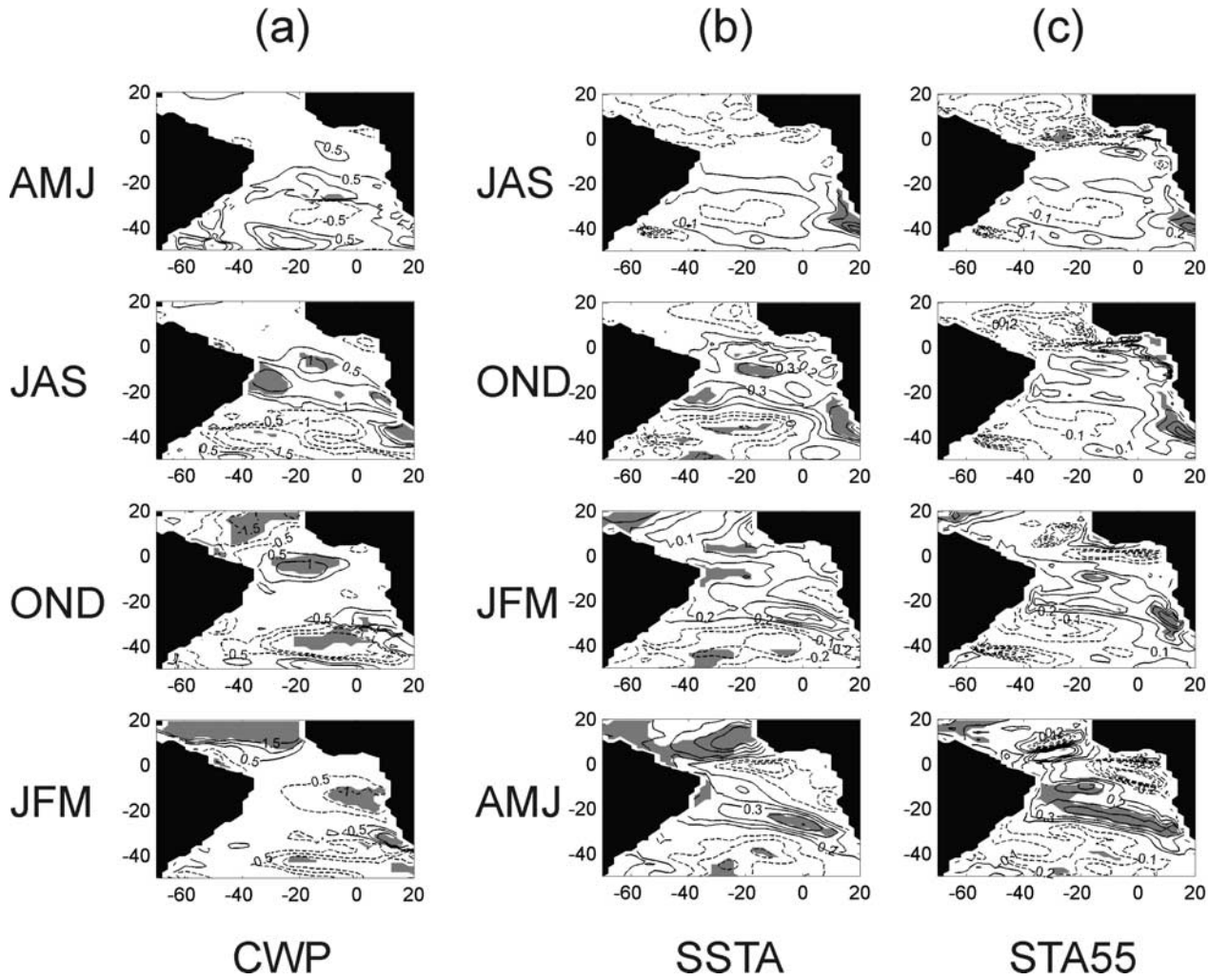

Figure 3. Seasonal composites of (a) CWP, (b) SSTA, and (c) STA55 for the El Niño phase. Positive (negative) CWP indicate areas where the wind stress anomalies and the wind stress climatology have the opposite (same) sign, thus favoring warm (cold) SSTA and STA55. Dashed (solid) contours denote negative (positive) values. Significant *t*-test areas at the 90% level are shaded (black and white version), and are marked by thick dashed lines (color version). The contour intervals are (Figure 3a) 0.5×10^{-2} N/m^2 and (Figures 3b and 3c) 0.1°C. The zero contour line is omitted. A color scale in °C is given on the right for each individual contour plot (color version). See color version of this figure in the HTML.

diately south of the equator are reduced (Figure 3a). Consistent with these CWP anomalies, large areas of tropical warming (midlatitude cooling) are apparent in Figure 3b. The temperature anomalies do not match exactly, and as shown below, other factors are also significant.

[26] During the mature phase (JFM), the cyclonic anomaly now south of Africa and the weak positive anomaly in the central to eastern South Atlantic (Figure 2a) lead to enhanced trade winds and westerlies (Figure 3a). As a result, negative temperature anomalies become apparent (Figures 3b and 3c) except for a band of warming extending northwest from the southern Benguela where the winds tend to be weaker than average.

[27] In general, the results of this section indicate that there is a one-season lag between the ocean temperature anomalies and the wind (CWP) forcing. This finding suggests that wind-driven surface flux changes may play a significant role in the evolution of upper ocean temperatures during El Niño in the South Atlantic.

4.1.3. Meridional Ekman Heat Transport (MEHT)

[28] The calculated MEHT anomalies are shown in Figure 4a. In AMJ, a positive MEHT anomaly is apparent from the subtropics to the equatorial South Atlantic. With respect to climatology, this anomaly weakens the generally negative (i.e., southward) transport that is apparent from the equator to about 25°S but strengthens the positive Ekman heat transport southward of 25°S. Hence there is a decrease in Ekman heat transport into the midlatitude South Atlantic from the tropics, consistent with relative warming in the 15°–25°S band seen a season later in JAS (Figure 3b). From 25°S to 40°S, the enhanced northward midlatitude MEHT contribute toward the cold temperature anomalies seen there in JAS (Figure 3b).

[29] During JAS, the positive MEHT anomaly in the tropical South Atlantic remains, thus supporting warming

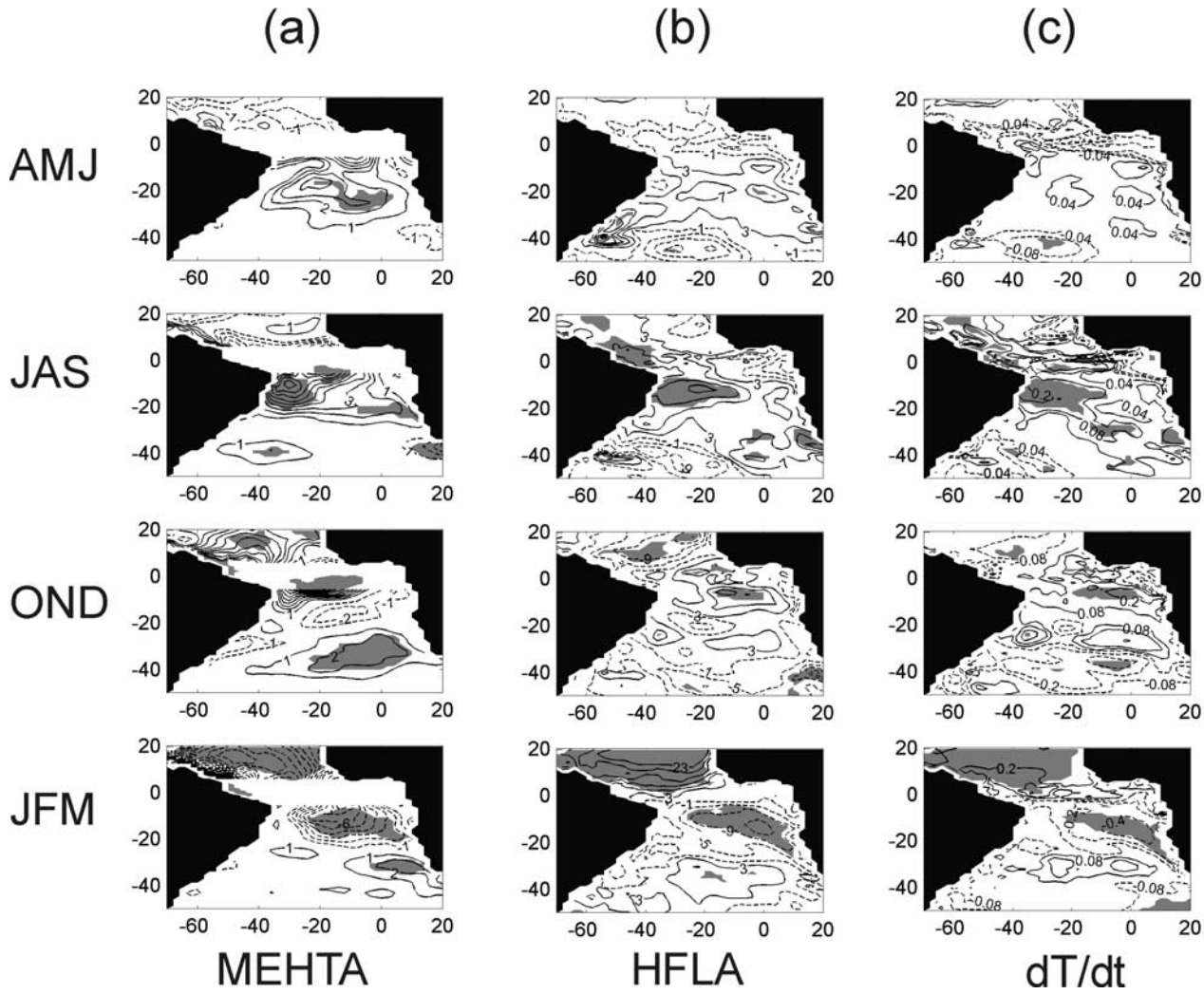

Figure 4. Seasonal composites of (a) meridional Ekman heat transport anomalies, where negative (positive) values indicate anomalous southward (northward) heat transport, (b) net surface heat flux, where negative (positive) values indicate flux out of (into) the ocean, and (c) expected temperature change. Dashed (solid) contours denote negative (positive) values. Significant *t*-test areas at the 90% level are shaded (black and white version), and are marked by thick dashed lines (color version). The contour intervals are (a) 1×10^3 W/m^2 and (b) 4 W/m^2. For Figure 4c the given contour intervals in °C are 0.2, 0.08, and 0.04 for AMJ/JAS and 0.4, 0.3, 0.2, and 0.1 for OND/JFM for negative and positive values, respectively. The zero contour line is omitted. A color scale in °C is given on the right for each individual contour plot (color version). See color version of this figure in the HTML.

there in OND due to a reduced southward heat transport. In the southwestern South Atlantic, a positive anomaly evolves (Figure 4b), enhancing the climatologically northward heat transport, and is thus consistent with the observed cold anomalies there in OND (Figure 3b). In the southern Benguela current region, the Ekman heat transport anomaly is negative, and supports the strong warming seen there in OND (Figure 3b).

[30] There is a less obvious agreement between the OND MEHT anomalies and the observed temperature anomalies a season later than was the case for the previous two seasons. A significant positive anomaly exists south of 25°S in OND and acts to enhance the northward heat transport, and thus supports midlatitude cooling in JFM (Figure 3b). The cold temperature anomaly that evolved in the northern Benguela region during JFM is consistent with the enhanced southward heat transport that is apparent in the subtropical South Atlantic.

[31] During JFM, the negative MEHT anomaly now extends from the equator to near 20°S (Figure 4a), strengthening the cold anomalies that extend northwestward from the northern Benguela region in AMJ (Figure 3b). Over, and west of, the southern Benguela, positive MEHT anomalies are apparent which contribute toward the warm anomalies seen here in AMJ (Figure 4a).

4.1.4. Net Downward Surface Heat Flux (HFL) and the Temperature Tendency

[32] During AMJ, the HFL anomalies shown in Figure 4b are positive in the central South Atlantic and negative in the midlatitudes and the equatorial region. Thus they mainly

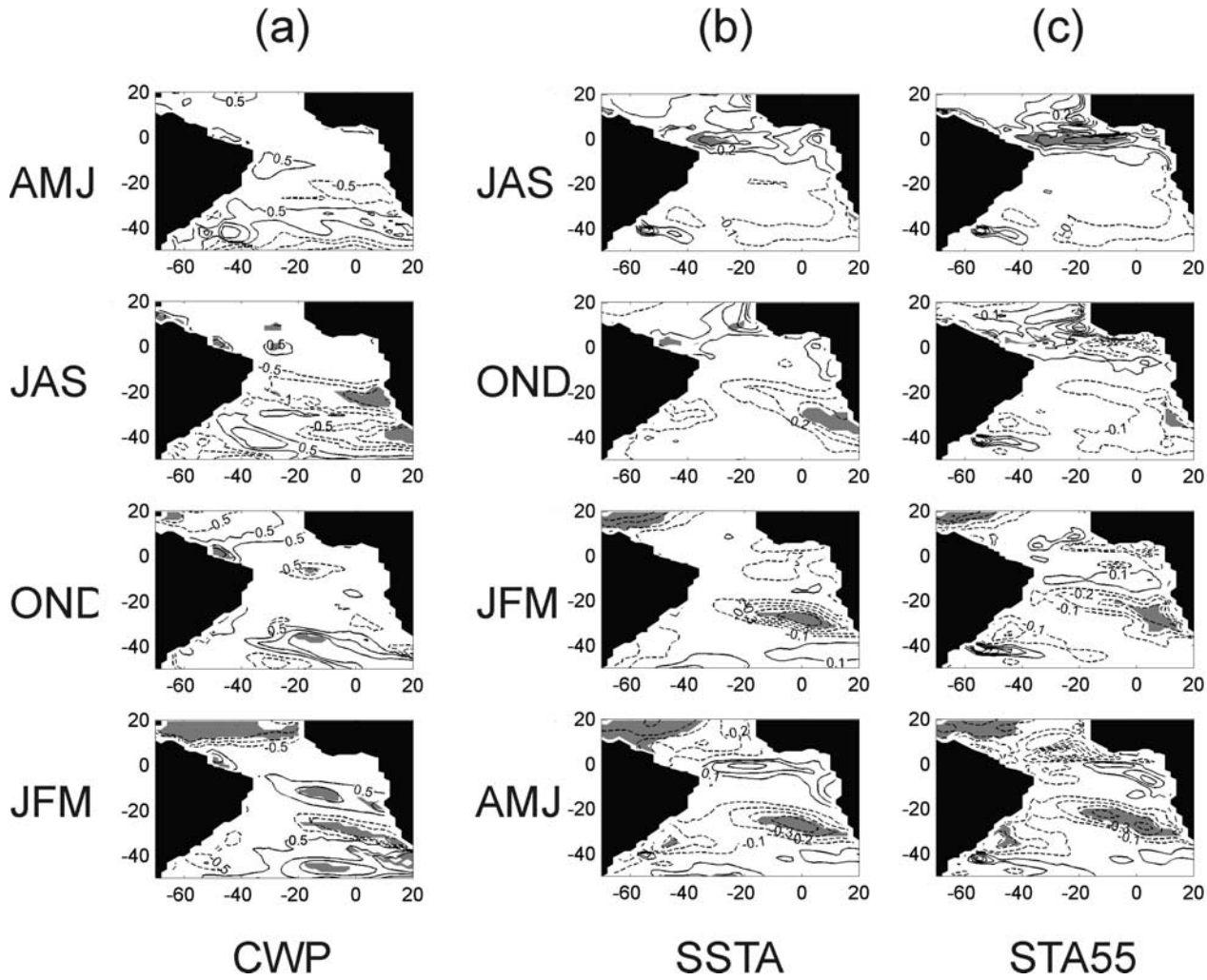

Figure 5. As for Figure 3 but for the La Niña phase. See color version of this figure in the HTML.

support the observed upper ocean temperatures occurring a season later in JAS (Figure 3b). The expected temperature changes due to these surface flux anomalies (Figure 4c) imply a weak warming over the tropics to subtropics, but underestimate the observed magnitude by about a factor of 10. The predicted temperatures in the equatorial region (Figure 4c) match much more closely with the observed ones (Figure 3b), as do those in the tropical North Atlantic. This result is consistent with the Ekman heat transport anomalies being important for the South Atlantic during JAS, as discussed above.

[33] Both the HFL anomalies in JAS and the expected temperature changes (Figures 4b and 4c) compare better to the observed OND ocean temperatures (Figure 3b). However, the magnitudes are still too low when compared to the actual temperature anomalies. Improved agreement occurs during the next OND and JFM season, especially in the southern subtropics/midlatitudes where cooling is apparent (Figure 3b).

4.1.5. Summary

[34] The El Niño phase is characterized by warmer upper ocean temperatures in the tropics and subtropics of the South Atlantic that reach their peak during OND of the El Niño year. Warming in the tropical North Atlantic occurs about one season later compared to the southern tropics. The midlatitude South Atlantic becomes significantly colder during OND of the El Niño year and JFM of the following year (mature phase) after which the negative anomalies begin to weaken.

[35] The South Atlantic subtropical anticyclone is generally weaker than usual during all of the El Niño year and the following mature phase, leading to a reduction in the southeasterly trades. As the negative SLP anomaly moves farther to the south, it tends to strengthen the midlatitude westerlies, thus inducing anomalous winds that affect the meridional Ekman heat fluxes. The southward tropical Ekman heat transport is reduced during AMJ to OND, favoring the observed warming in the tropics and parts of the subtropics. On the other hand, the northward midlatitude Ekman heat transport is enhanced, consistent with the observed cooling in the midlatitudes.

[36] Surface heat flux anomalies contribute to the evolution of the upper ocean temperature anomalies. This can be seen most clearly in OND and JFM, where the calculated temperature changes match reasonably well with the model

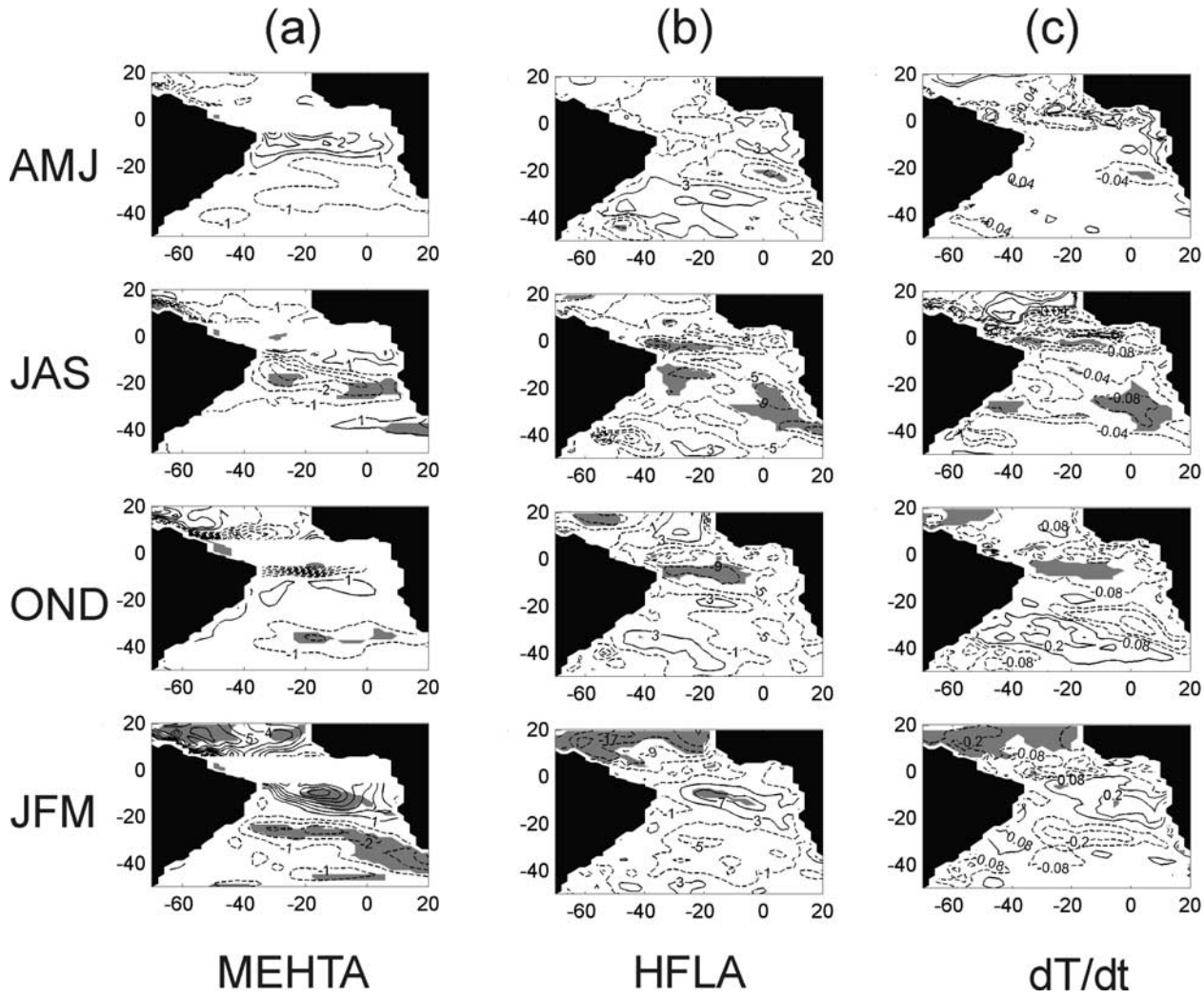

Figure 6. As for Figure 4 but for the La Niña phase. See color version of this figure in the HTML.

temperature anomalies one season later. There is an increased heat flux into the ocean mainly over the tropics, subtropics, and the Benguela current region in AMJ, JAS, and to a lesser extent, OND. Reduced heat fluxes are apparent over parts of the midlatitudes consistent with cool temperatures there.

4.2. Detailed Analysis of the La Niña-Induced Anomalies

4.2.1. Upper Ocean Temperatures

[37] Figures 5b and 5c show the model SST and ST55 anomalies for the La Niña phase. In JAS, one center of cold anomalies lies in the southern Benguela current region. It becomes significant at the 90% level and moves northward during the following OND, JFM, and AMJ. In JFM, these cool anomalies peak in the central and eastern subtropics with weaker cooling apparent over most of eastern tropics. The midlatitudes are cold in JAS, but these cool anomalies disappear in the mature phase (JFM) and AMJ. The eastern equatorial South Atlantic is warm in JAS, but these anomalies weaken in OND and become mainly negative anomalies by JFM. In AMJ, a reversal to mainly warm anomalies here is apparent in the equatorial region and southeastern tropics.

4.2.2. Sea Level Pressure (SLP) and CWP

[38] Figure 2b shows the global SLP anomalies during La Niña. Over the South Atlantic, a positive SLP anomaly is apparent in AMJ in the subtropics/midlatitudes. This feature weakens during JAS but becomes stronger and significant again during OND and JFM as the well-known cyclonic anomalies become more established over the tropical Indo-Pacific. The SLP evolution is more or less opposite to that shown in Figure 2a for the El Niño and essentially shows the reverse phase Pacific South American pattern over the South Pacific/South Atlantic region. It should be noted that the positive anomalies are farther south than the corresponding cyclonic anomalies during El Niño (Figure 2a) so they correspond more to a weakening of the midlatitude westerly belt in the South Atlantic rather than a strengthening of the anticyclone.

[39] The evolution in CWP and upper ocean temperatures (Figure 5) is again more or less the reverse in pattern to that seen for the El Niño, so a detailed discussion is not

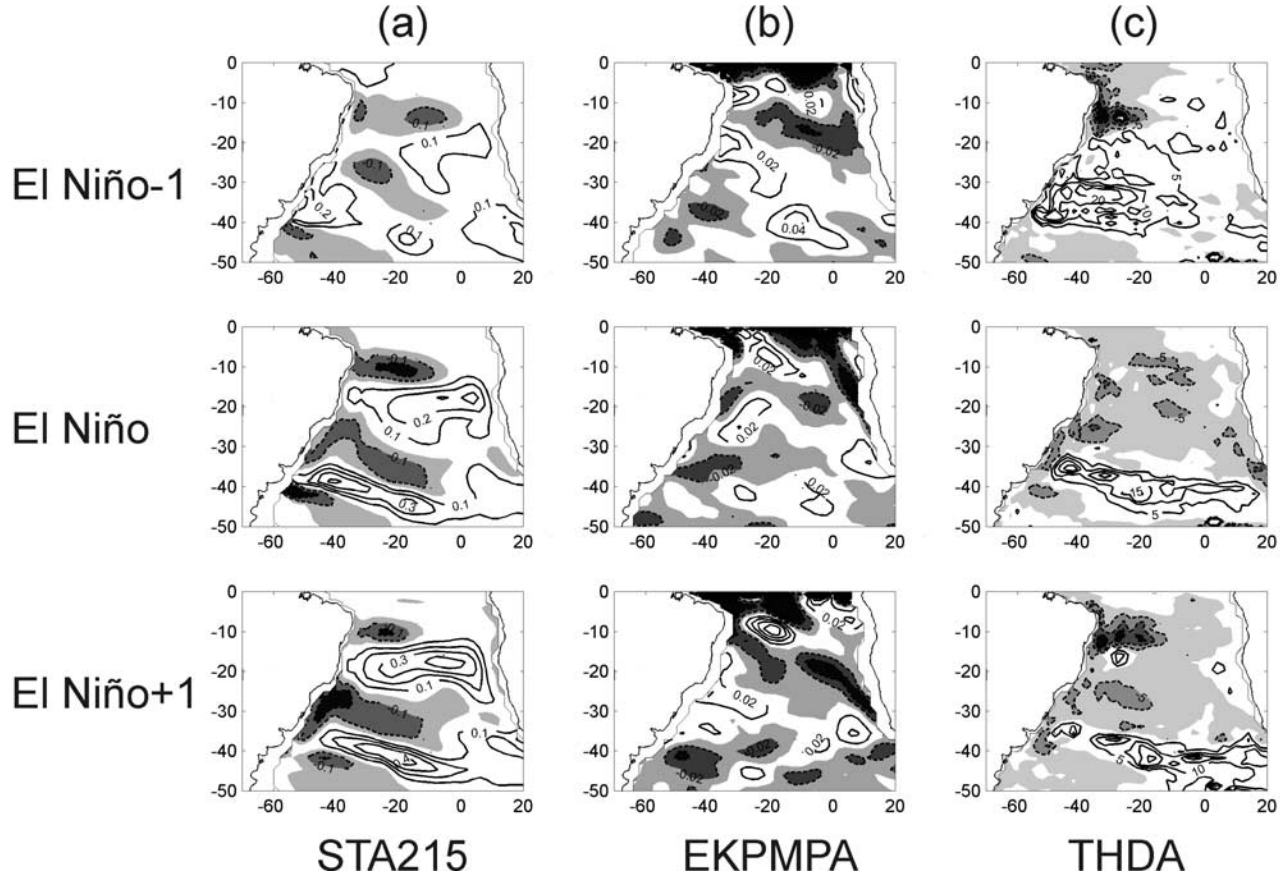

Figure 7. Annual means of (a) STA215, (b) Ekman pumping anomalies where negative (positive) values indicate downwelling (upwelling), and (c) thermocline depth anomalies where negative (positive) values indicate a shallower (deeper) thermocline for the El Niño-1 to El Niño+1 years. Dashed (solid) contours denote negative (positive) values. Negative values are shaded for clarity (black and white version). The contour intervals are (a) 0.1°C, (b) 0.02 m/s, and (c) 5 m. The zero contour line is omitted. A color scale in °C is given on the right for each individual contour plot (color version). See color version of this figure in the HTML.

provided. Thus there is a one-season lag between the wind changes and the upper ocean temperature response. However, the magnitudes of the anomalies are not always the same as those seen in Figure 3 for the El Niño, suggesting that the relationship between the ENSO forcing and the South Atlantic response is not necessarily linear.

[40] Generally speaking, the agreement between the CWP fields and the observed upper ocean temperature fields is not as clear during La Niña as it is during El Niño. Nevertheless, the significant temperature anomalies (mainly in, and northwest of, the southern Benguela current region) are supported by the anomalous winds.

4.2.3. Meridional Ekman Heat Transport (MEHT), Net Downward Surface Heat Flux (HFL), and Temperature Tendency

[41] With the exception of AMJ, the MEHT anomalies (Figure 6a) are roughly the reverse of the El Niño ones (Figure 4a). They tend to be negative during AMJ, OND, and JFM in the midlatitudes, and during AMJ, JAS, and JFM in the subtropics. Positive anomalies are apparent mostly in the tropical region in AMJ, JAS, and JFM. The negative anomalies in the midlatitudes (subtropics) reduce (enhance) the mean northward (southward) Ekman heat transport. They are therefore consistent with the dissipation of the JAS cool anomaly near 40°S by JFM and the maintaining of the cool anomalies in the subtropics. The positive MEHT anomalies in the tropics during AMJ, JAS, and JFM favor warming over the tropical and eastern tropical South Atlantic a season later.

[42] The heat flux anomalies for AMJ and the calculated temperature changes (Figures 6b and 6c) show some similarities in pattern over the South Atlantic (except the southwest and equatorial regions), with the observed model temperature anomalies one season later (JAS). Better agreement is seen between the JAS heat flux anomalies/temperature tendencies and the OND temperature anomalies (Figures 6b and 6c and Figures 5b and 5c) over most of the South Atlantic. This improvement continues for OND and JFM when the calculated temperature changes are consistent with most of the model upper ocean temperature characteristics. However, as for the El Niño case, the calculated temperatures are typically too low in magnitude when compared to the actual model temperature anomalies.

4.2.4. Summary

[43] During La Niña, the upper ocean temperatures are generally colder than average over most of the basin except

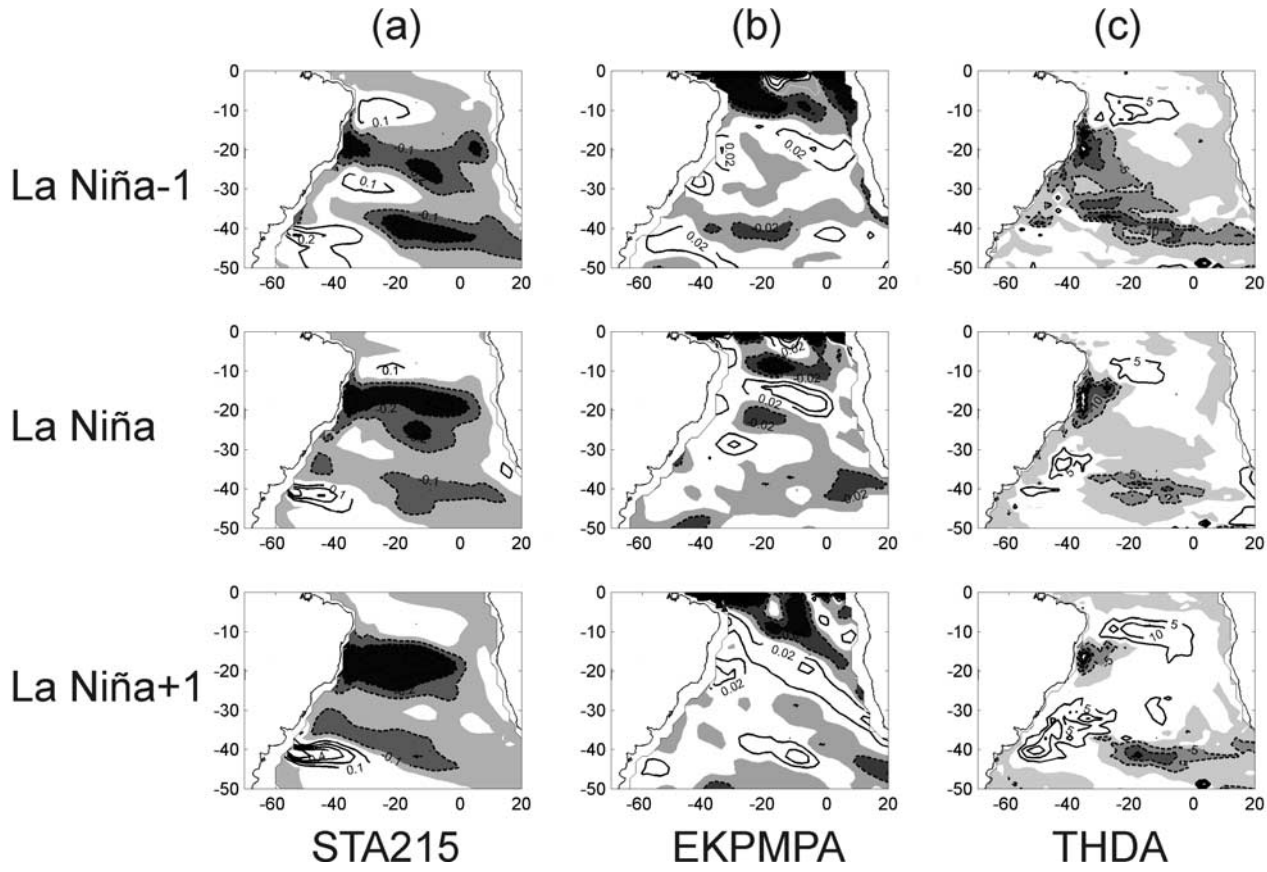

Figure 8. As for Figure 7 but for La Niña composites. See color version of this figure in the HTML.

the tropical southeast Atlantic and the midlatitudes in AMJ. As in the El Niño case, the anomalies show a northward movement with the northern tropical response appearing to lag that in the southern tropics by about a season. The midlatitude westerly belt over the South Atlantic is generally weaker and, to a lesser extent, the subtropical anticyclone stronger during La Niña, enhancing the trades, thus favoring cooling. These winds lead to changes in the net surface heat fluxes which are in broad agreement with the model temperature anomalies. Changes in the meridional Ekman heat transport are also seen to contribute, particularly in the tropical southeast Atlantic and the midlatitudes.

5. Subsurface Temperature Anomalies STA215

5.1. Patterns

[44] Temperature patterns at 215 m depth (STA215) associated with ENSO were also examined and found to not vary much with the season. Therefore, annual mean ENSO composites are shown for the El Niño −1, 0, and +1 years (Figure 7) and La Niña −1, 0, and +1 years (Figure 8). During the El Niño −1 to 1 year (Figure 7), the anomaly pattern consists of two warm anomalies, one situated near the center of the subtropical gyre (15°–30°S), and the other stretching southeastward from the midlatitude South American coast to south of Africa. The equatorward and poleward margins of the subtropical gyre tend to show cold anomalies, as does the far southwest. During La Niña (Figure 8), the pattern reverses sign to some extent, although cool anomalies tend to dominate, again pointing to nonlinearity between the El Niño and La Niña response.

[45] Figures 7 and 8 suggest that there is a subsurface signal in the South Atlantic related to El Niño and La Niña. Although the pattern remains quite stable in shape and intensity, there is variability; the warm anomaly in the center of the basin increases during the El Niño-1 year to the El Niño+1, as does the corresponding cold anomaly during the La Niña-1 to the La Niña +1 year. The tropical cold anomaly increases during the El Niño year but decreases after that.

5.2. Mechanisms

[46] Since the STA215 patterns do not change a great deal during the −1 to +1 years in both the El Niño and La Niña case, the forcing for these patterns is likely to be steady on at least annual timescales. If the potential forcing shows any evidence of altering the STA215 from year to year, then it would be apparent in their annual means. Thus the following analyses are based on annual means. Changes in thermocline depth are known to have an impact on temperature in the upper and lower ocean levels. An increasing (decreasing) thermocline depth can lead to a warmer (cooler) ocean at shallower levels. Upwelling and downwelling and associated divergence and convergence also modify upper and lower level temperatures. The thermocline itself may be altered by wind-driven upwelling or downwelling but also by heat loss to the atmosphere, which implies convection.

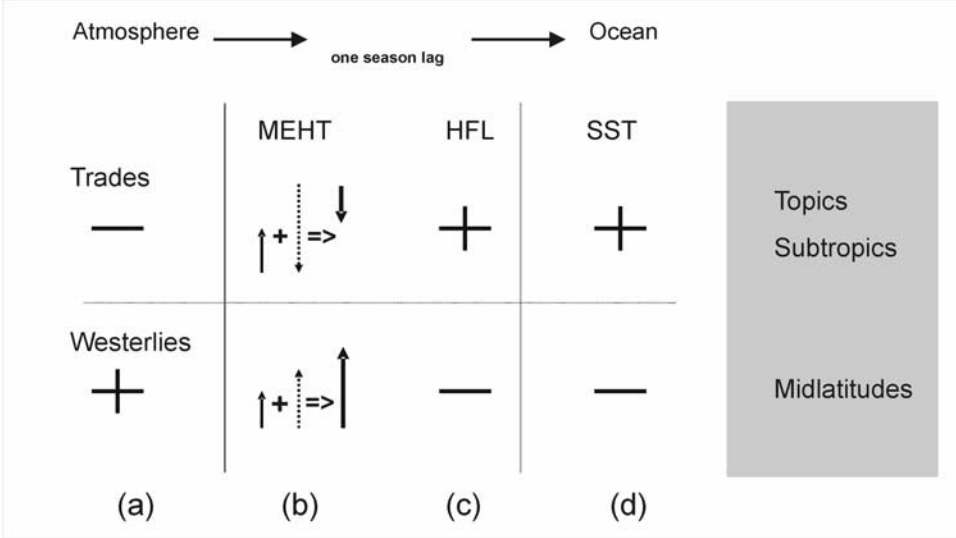

Figure 9. Schematic picture of the South Atlantic response to El Niño. (a) Weaker trades (stronger westerlies) lead to (b) reduced tropical southward (enhanced midlatitude northward) meridional Ekman heat transports (thin arrow denotes the anomaly, dotted arrow denotes the climatology, and thick arrow denotes the resulting Ekman heat transport) and (c) positive (negative) net surface heat fluxes. These anomalies favor (d) upper ocean warming (cooling) in the tropics to subtropics (midlatitudes).

[47] Ekman pumping patterns and thermocline depth anomalies (Figure 7) show some features that can help explain the STA215. The upwelling cells in the El Niño and El Niño +1 year near 10°S correspond well with the tropical cold anomaly in the STA215, although some advection by the equatorial currents is apparent. South and north of that, downwelling is evident which coincides with the observed warm anomaly near 20°S and, in El Niño −1, also at 0°–5°S. The warm anomaly at 35°–40°S matches reasonably well with downwelling cells existing during the 3 years. The cold anomaly at 20°–30°S may be linked to some extent with upwelling cells in the west.

[48] The thermocline depth (Figure 7) gives further support for the cold STA215 near 10°S since it shows regions of decreased thermocline depth in all 3 years in the tropical western Atlantic. During the El Niño and to lesser extent El Niño+1 year, this region of decreased depth spreads over most of the tropics and subtropics consistent with the mainly cool anomalies evident. An exception is the warming near 15°–20°S; this area does show some areas with small increases in thermocline depth at its western and eastern margins during the El Niño and El Niño+1 years but a mainly shallower thermocline in the center of this latitude zone, suggesting that this region is mainly responding to the strong downwelling from the upper layers. The area of increased thermocline depth near 30°–35°S moves southeast in the El Niño year and farther east in the El Niño+1 year consistent with the band of midlatitude warming in these years. The southwestern cold anomaly near 40°–45°S coincides with a shallower thermocline during each year.

[49] During La Niña, many of the previously described features are the same, but with reversed signs. Thermocline depth and Ekman pumping anomalies (Figure 8) both imply warm STA215 near 10°S throughout the La Niña years. Large areas of shallower thermocline and upwelling are apparent over the subtropics in the −1 and 0 years, leading to reduced STA215. In the +1 year, the region of cooling is more obvious in the western and central subtropics, mainly consistent with the other fields. In the midlatitudes near 35°–40°S, there are areas of Ekman suction and shallower thermocline (particularly in the −1 and +1 years) that match with parts of the band of cool STA215. This correlation is also seen between the warm STA215 in the southwest and the increased thermocline depth for the La Niña 0 and +1 years. In all cases, however, there is not an exact match between the STA215 anomalies and those in the thermocline depth or Ekman pumping due to advection by the mean currents. Examples of such advection can be seen in the Brazil/Malvinas Current confluence region in the southwest and the South Atlantic Current region across the basin near 40°S.

[50] The results suggest that Ekman pumping may significantly influence the thermocline depth, and hence subsurface temperatures, in the South Atlantic. In turn, these Ekman pumping anomalies derive from the wind stress anomalies, leading to a time-filtered signal from the overlying atmosphere on the subsurface South Atlantic Ocean. Previous work [e.g., *Reason et al.*, 1987] suggests that there is a robust annual period Rossby wave signal in this basin, particularly in the southeast Atlantic. Rossby waves may also play a role in influencing the subsurface temperatures, and, to investigate this, Hovmueller plots (both meridional and zonal with time; not shown) were constructed of anomalies in thermocline depth, subsurface temperature, and sea surface height for the 1949–1999 period. However, although Rossby wave signals are apparent during this period, no obvious modulation of these features by ENSO was evident. This lack of a coherent signal may occur because the changes in the SLP and winds during ENSO

(Figure 2) described above are rather complex in pattern, suggesting that a coherent and obvious Rossby wave modulation will not be easy to detect.

6. Discussion and Conclusions

[51] Seasonal composites of upper ocean temperature, SLP, wind stress, meridional Ekman heat transport, and net surface heat flux anomalies presented herein suggest that during ENSO, upper ocean temperatures in the South Atlantic are significantly influenced by the ENSO-induced wind stress anomalies. Figure 9 shows a schematic picture of the processes that lead to temperature changes during El Niño events in the South Atlantic. During the El Niño onset, the global SLP teleconnection pattern implies a negative SLP anomaly in the South Atlantic region via the Pacific South America pattern [*Mo and Paegle*, 2001]. Its main effects are the weakening of the southeasterly trades (mainly during AMJ and JAS of the onset year) and a strengthening of the midlatitude westerlies (particularly from JAS to the following JFM mature phase). As a result, the southward tropical (northward midlatitude) Ekman heat transport is reduced (enhanced), thus favoring warming over the South Atlantic from the equator to about 25°S and cooling in the midlatitudes, with about a one-season lag. The wind anomalies lead to changes in the net surface heat fluxes that are generally consistent with the observed changes in the model upper ocean temperatures one season later. Examination of the NCEP latent heat fluxes suggests that evaporation is the major contributor to the net surface heat flux, consistent with *Sterl and Hazeleger* [2003]. During La Niña, the upper ocean temperature changes and the associated mechanisms are roughly the reverse of those evident during El Niño. The patterns are not exactly opposite, suggesting some nonlinearity to the response.

[52] The mechanisms leading to temperature changes during El Niño (La Niña) in the tropical South Atlantic are comparable to those that cause warming (cooling) in the northern tropics, i.e., a weakening (strengthening) of the trades and associated changes in surface heat fluxes [*Huang et al.*, 2002; *Giannini et al.*, 2001]. Furthermore, the results from the ORCA model suggest that the warm (cold) ENSO signal reaches the South Atlantic region via an atmospheric teleconnection pattern, one season in advance (i.e., in OND), in comparison with the North Atlantic.

[53] Annual means of Ekman pumping anomalies and thermocline depth anomalies are broadly consistent with the observed near-thermocline ocean temperature anomalies with some advection of the response by the mean currents. They imply subsurface temperature changes due to atmospheric forcing since the Ekman pumping anomalies are derived from the wind stress anomalies. It is possible that Rossby wave generation via these wind stress anomalies could contribute; however, an investigation showed that although such waves are prominent during the 52 years of model output, no obvious modulation of their characteristics during ENSO could be found.

[54] The results of this study suggest that there is a coherent and significant ENSO impact on the South Atlantic that extends from low to midlatitudes, and that the ORCA model may be used to diagnose in more detail the evolution of this impact and the processes involved. Modulations of the South Atlantic anticyclone and associated trade winds and westerlies, suggested here as part of the PSA pattern, are important for the evolution of the anomalies. Modulations of the anticyclone are also very important for the leading South Atlantic climate mode [e.g., *Venegas et al.*, 1996] as well as Benguela warm and cool events [*Florenchie et al.*, 2003]. Thus, better monitoring of the anticyclone region and its associated surface fluxes should be a high priority for improving our understanding of South Atlantic climate variability.

[55] **Acknowledgments.** Funding from the DAAD (German Academic Exchange Service) is gratefully acknowledged. We would like to thank the NOAA CIRES Climate Diagnostic Center, Boulder, Colorado, for providing the data for some of the images shown.

References

Binet, D., B. Gobert, and L. Maloucki (2001), El Niño-like warm events in the Eastern Atlantic (6°N, 20°S) and fish availability from Congo to Angola (1964–1999), *Aquat. Living Resour.*, *14*, 99–113.

Blanke, B., and P. Delecluse (1993), Variability of the tropical Atlantic Ocean simulated by a general circulation model with two different mixed layer physics, *J. Phys. Oceanogr.*, *23*, 1363–1388.

Fichefet, T., and M. A. Morales Maqueda (1997), Sensitivity of a global sea ice model to the treatment of ice thermodynamics and dynamics, *J. Geophys. Res.*, *92*, 12,609–12,646.

Florenchie, P., J. R. E. Lutjeharms, and C. J. C. Reason (2003), The source of Benguela Niños in the South Atlantic Ocean, *Geophys. Res. Lett.*, *30*(10), 1505, doi:10.1029/2003GL017172.

Gammelsrod, T., C. H. Bartholomae, D. C. Boyer, V. L. L. Philipe, and M. J. O'Toole (1998), Intrusion of warm surface layer along the Angolan-Namibian coast on February–March: The 1995 Benguela Niño, *S. Afr. J. Mar. Sci.*, *19*, 41–56.

Gent, P. R., and J. C. McWilliams (1990), Isopycnal mixing in ocean circulation models, *J. Phys. Oceanogr.*, *20*, 150–156.

Giannini, A., J. C. H. Chiang, M. A. Cane, Y. Kushnir, and R. Seager (2001), The ENSO teleconnection to the tropical Atlantic Ocean: Contribution of the remote and local SSTs to rainfall variability in the tropical Americas, *J. Clim.*, *14*, 4530–4544.

Huang, B., P. S. Schopf, and Z. Pan (2002), The ENSO effect on the tropical Atlantic variability: A regionally coupled model study, *Geophys. Res. Lett.*, *29*(21), 2039, doi:10.1029/2002GL014872.

Kalnay, E., et al. (1996), The NCEP/NCAR, 40-Year Reanalysis Project, *Bull. Am. Meteorol. Soc.*, *77*(3), 437–471.

Lentini, C. A. D., G. G. Podesta, E. J. S. Campos, and D. B. Olson (2001), Sea surface temperature anomalies on the Western South Atlantic from 1982 to 1994, *Cont. Shelf. Res.*, *21*, 89–112.

Levitus, S. (1987), Zonally integrated meridional Ekman heat fluxes for the world ocean and individual ocean basins, *J. Phys. Oceanogr.*, *17*, 1484–1492.

Levitus, S. (1998), *World Ocean Atlas 1998*, Natl. Oceanic and Atmos. Admin., Silver Spring, Md.

Madec, G., P. Delecluse, M. Imbard, and C. Levy (1998), OPA 8.1 Ocean General Circulation Model reference manual, *Notes Pole de Model. 11*, 91 pp., Inst. Pierre-Simon Laplace, Paris.

Melice, J.-L., and L. Servain (2003), The tropical Atlantic meridional SST gradient index and its relationships with the SOI, NAO and Southern Ocean, *Clim. Dyn.*, *20*, 447–464.

Mo, K. C., and J. N. Paegle (2001), The Pacific-South American modes and their downstream effects, *Int. J. Climatol.*, *21*, 1211–1229.

Palastanga, V. S., C. S. Vera, and A. R. Piola (2002), On the leading modes of sea surface temperature variability on the South Atlantic Ocean, *CLIVAR Exchanges*, *7*(3–4), 12–15.

Rayner, N. A., E. B. Horton, D. E. Parker, C. K. Folland, and R. B. Hackett (1996), *Clim. Res. Tech. Note 74*, MetOffice, Bracknett, UK.

Reason, C. J. C. (2000), Multidecadal climate variability in the subtropics/mid-latitudes of the Southern Hemisphere oceans, *Tellus, Ser. A*, *52*, 203–223.

Reason, C. J. C., L. A. Mysak, and P. F. Cummins (1987), Generation of annual period Rossby waves in the South Atlantic Ocean by the wind stress curl, *J. Phys. Oceanogr.*, *17*, 2030–2042.

Reason, C. J. C., M. Rouault, J.-L. Melice, and D. Jagadeesha (2002), Winter rainfall variability in SW South Africa and large scale ocean-atmosphere interactions, *Met. Atmos. Phys.*, *80*(1–4), 19–29.

Robertson, A. W., J. D. Farrara, and C. R. Mechoso (2003), Simulations of the atmospheric response to South Atlantic sea surface temperature anomalies, *J. Clim.*, *16*, 2540–2551.

Rouault, M., P. Florenchie, N. Fauchereau, and C. J. C. Reason (2003), Southeast tropical Atlantic warm events and southern African rainfall, *Geophys. Res. Lett.*, *30*(5), 8009, doi:10.1029/2002GL014840.

Schmitz, W. J. (1995), On the inter-basin scale thermohaline circulation, *Rev. Geophys.*, *33*, 151–173.

Smith, W. H. F., and D. T. Sandwell (1997), Global sea floor topography from satellite altimetry and ship depth soundings, *Science*, *277*, 1956–1962.

Stammer, D., R. Tokmakian, A. Semtner, and C. Wunsch (1996), How well does a 1/4° model simulate large-scale oceanic observations?, *J. Geophys. Res.*, *101*(C11), 25,779–25,812.

Sterl, A., and W. Hazeleger (2003), Coupled variability and air-sea interaction in the South Atlantic Ocean, *Clim. Dyn.*, *21*, 559–571.

Venegas, S. A., L. A. Mysak, and D. N. Straub (1996), Evidence for interannual and interdecadal climate variability in the South Atlantic, *Geophys. Res. Lett.*, *23*(19), 2673–2676.

Venegas, S. A., L. A. Mysak, and D. N. Straub (1997), Atmosphere-ocean coupled variability in the South Atlantic, *J. Clim.*, *10*, 2904–2920.

Venegas, S. A., L. A. Mysak, and D. N. Straub (1998), An interdecadal climate cycle in the South Atlantic and its links to other ocean basins, *J. Geophys. Res.*, *103*(C11), 24,723–24,736.

Wainer, I., and S. A. Venegas (2001), South Atlantic multidecadal variability in the Climate System Model, *J. Clim.*, *15*, 1408–1420.

F. Colberg and C. J. C. Reason, Oceanography Department, University of Cape Town, Private Bag, Rondebosch 7701, South Africa. (colberg@ocean.uct.ac.za)

K. Rodgers, Laboratoire d'Oceanographie Dynamique et de Climatologie, CNRS, University Paris VI, 4 Place Jussieu, Paris F-75252, France.